



ELSEVIER

Available online at [www.sciencedirect.com](http://www.sciencedirect.com)

International Journal of Rock Mechanics &amp; Mining Sciences 45 (2008) 467–477

---



---

International Journal of  
**Rock Mechanics  
and Mining Sciences**


---



---

[www.elsevier.com/locate/ijrmms](http://www.elsevier.com/locate/ijrmms)

# Micromechanical modelling of anisotropic damage in brittle rocks and application

Qizhi Zhu, Djimedo Kondo, Jianfu Shao\*, Vincent Pensee<sup>1</sup>

*Laboratory of Mechanics of Lille, UMR 8107CNRS, USTL, Cite Scientifique, 59655 Villeneuve d'Ascq, France*

Received 4 November 2006; received in revised form 25 June 2007; accepted 2 July 2007

Available online 6 September 2007

---

## Abstract

The present study deals with the formulation of a new micromechanical model for anisotropic damage in brittle rocks and its numerical implementation and application. The basic idea is to integrate Eshelby solution-based homogenization approaches into the standard thermodynamics framework for the description of inelastic deformation contributed by microcracks; the anisotropic damage is coupled with frictional sliding which occurs on closed cracks. The identification of the micromechanical model requires only six parameters, each with a clear physical meaning. Comparisons of the model's predictions with experimental data are performed on both conventional and true triaxial compression paths, respectively, for two granites. The proposed model is implemented into the finite element software Abaqus. Its application to an underground excavation problem shows that the proposed model is able to describe general responses and damaged zone evolution due to excavation.

© 2007 Elsevier Ltd. All rights reserved.

*Keywords:* Damage; Micromechanics; Brittle rocks; Microcracks; Fracture; Anisotropy

---

## 1. Introduction

Damage by microcrack growth is commonly considered as the main mechanism of inelastic deformation and failure in brittle materials such as concrete and rocks. A number of experimental investigations have shown different modes of initiation and propagation of microcracks in rock materials [1–8]. There are generally two dissipation mechanisms, respectively related to the size evolution of microcracks and frictional sliding in closed cracks, to be taken into account in modelling of damage. Consequences of damage by microcrack growth mainly include nonlinear stress–strain relations, deterioration of elastic properties, induced anisotropy, irreversible deformation after unloading, dilatancy, hysteric response and unilateral effects. Further, induced damage can also affect transport and diffusion properties, in particular permeability. Indeed, rock permeability can significantly increase due to propa-

gation of microcracks and associated volumetric dilatancy [9–14]. However, in this paper, only mechanical modelling of anisotropic damage will be addressed.

The modelling of induced anisotropic damage is classically performed by means of macroscopic continuum damage models (CDM). In these models, internal variables (scalar, vector, second-order tensor and even higher rank tensors) are used to describe the state of damage. A damage evolution law is then formulated as a function of stress or strain, using the framework of irreversible thermodynamics or some principles of linear fracture mechanics, for instance [15–22] just to mention a few. The main advantage of CDM is the ability to provide macroscopic constitutive equations which can be easily implemented in computer codes and applied to engineering analysis. However, some assumptions used in these models are not clearly based on physical mechanisms involved in microcrack growth, for instance, the so-called effective stress concept. Further, despite the numerical efficiency of this approach, there remain some critical issues which need more physical and mathematical analysis, for example unilateral effects related to crack closure and coupling

---

\*Corresponding author. Tel./fax: +33 3 20434626.

E-mail address: [jian-fu.shao@polytech-lille.fr](mailto:jian-fu.shao@polytech-lille.fr) (J. Shao).

<sup>1</sup>Now at the University of Marne-la-Vallée, France.

between damage and friction sliding. The mathematical description of these phenomena could be quite complex.

On the other hand, significant advances have been realized in micromechanical modelling of damage in brittle materials, providing a new way for a more physically based description of anisotropic damage by taking into account progressive evolution of microstructure at grain scale [23,24]. Various micromechanical models have been proposed for concrete and rocks [25–27] just to mention a few. Most of these models do not use an Eshelby-type rigorous homogenization procedure to define macroscopic behaviour of heterogeneous material from microscopic considerations. As a consequence, effects of special crack distribution cannot be properly described [28]. Moreover, these models are often limited to dilute distributions of microcracks, without interaction. Another aspect, which is important for damage modelling in brittle rocks, is the coupling between damage and frictional sliding in closed cracks leading to volumetric dilatancy. This one is generally not properly considered in the previous models.

In this paper, we propose the formulation of a new micromechanical model for anisotropic damage coupled with frictional sliding for brittle rocks and its numerical implementation for structural analysis. This model is based on a rigorous micro–macro approach for heterogeneous materials. The basic idea is to incorporate Eshelby-solution-based homogenization techniques into the standard thermodynamics framework for the description of damage by microcracks. The Eshelby-type homogenization techniques provide a general micromechanics background for damage modelling in which the crack spatial distribution can also be described [29,30]. The thermodynamics framework gives a standard procedure for the formulation of damage evolution law and the numerical implementation of the model. The emphasis will be put on the coupling between damage and frictional phenomena which allows explaining the salient features of brittle behaviours of rocks under compressive loadings. For this purpose, it comes from the micromechanical analysis that the crack density parameter [31] in each space orientation and two kinetic variables (sliding and opening along crack surface) allow describing inelastic deformation contributed by microcracks. Furthermore, a damage energy release rate-based criterion is proposed to describe the evolution of crack size. The transition condition of crack opening/closure will also be discussed. Comparisons of the model's predictions with experimental data are performed on both conventional and true triaxial compression paths, respectively, for two granites. The proposed micromechanical model is then implemented in the finite element software Abaqus with UMAT facility. Its application to an underground excavation problem shows a good agreement between numerical results and in situ data concerning radial displacements and evolution of damaged zone.

Throughout the paper, the following notations tensor products of any second-order tensors **A** and **B** will be used:  $(\mathbf{A} \otimes \mathbf{B})_{ijkl} = A_{ij}B_{kl}$ ,  $(\mathbf{A} \underline{\otimes} \mathbf{B})_{ijkl} = A_{ik}B_{jl} + A_{il}B_{jk}$ . The tensor

product of two vectors  $\underline{a}$  and  $\underline{b}$  is denoted  $(\underline{a} \otimes \underline{b})_{ij} = a_i b_j$  and its symmetric part  $(\underline{a} \underline{\otimes} \underline{b})_{ij} = \frac{1}{2}(a_i b_j + a_j b_i)$ . With second rank identity tensor  $\delta$ , the usually used fourth order isotropic tensors  $\mathbb{I}$  and  $\mathbb{J}$  are expressed as  $\mathbb{I}_{ijkl} = \frac{1}{2}(\delta_{ik}\delta_{jl} + \delta_{il}\delta_{jk})$  and  $\mathbb{J}_{ijkl} = \frac{1}{3}\delta_{ij}\delta_{kl}$ , respectively.

## 2. Macroscopic free energy of cracked material

The micromechanical approach aims to study effective material properties at macroscopic scale based on information at micro scale. For this purpose, the cracked material is considered as a heterogeneous composite with a matrix phase weakened by microcracks. A representative elementary volume (REV), denoted by  $\Omega$  and having a boundary surface  $\partial\Omega$ , is adopted, as shown in Fig. 1.

In the present study, the REV is composed of an isotropic linear elastic matrix with stiffness  $\mathbb{C}^s$  and of a distribution of microcracks with the elasticity tensor  $\mathbb{C}^c$  ( $\mathbb{C}^c = 0$  in its opening state in order to account for the cancellation of the local stress  $\sigma^c$  on open crack faces). Thus, the REV may be considered as a matrix-inclusion system and the micromechanical analysis based on the fundamental solution of Eshelby [32,33].

In this paper, microcracks are assumed to be penny-shaped. A family of cracks is characterized by its normal  $\underline{n}$ , radius  $a$  and the half opening  $c$  (Fig. 2). The aspect ratio  $\varepsilon = c/a$  of such penny-shaped cracks is such that  $\varepsilon \ll 1$  (Fig. 2). The volume fraction of cracks  $\varphi^c$  is expressed as:

$$\varphi^c = \frac{4}{3}\pi a^2 c \mathcal{N} = \frac{4}{3}\pi \varepsilon d, \quad (1)$$

where  $\mathcal{N}$  denotes the crack density (number of cracks per unit volume) of the considered family of cracks and  $d = \mathcal{N}a^3$  is the crack density parameter as initially introduced by Budiansky and O'Connell [31] and widely used as an internal damage variable in micromechanical analysis [34].

The related displacement jump between the two cracks faces is noted by  $[\underline{u}]$ . The unilateral contact conditions of

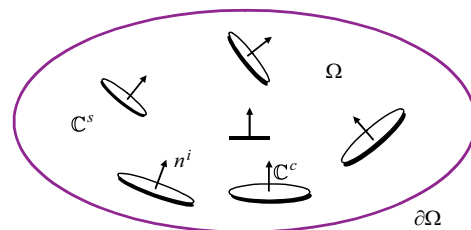


Fig. 1. Representative elementary volume in microcracked solids (REV).

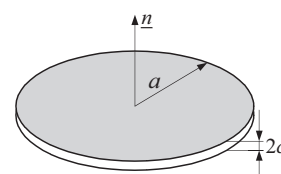


Fig. 2. Schematic representation of a penny-shaped crack.

the cracks are described as

$$[u_n] \geq 0, \sigma_n^c \leq 0, [u_n] \sigma_n^c = 0 \quad (2)$$

with  $\sigma_n^c$  as the normal component of the local stress field and  $[u_n]$  the normal component of the displacement jump  $[u]$ .

We consider now a macroscopic uniform stress,  $\Sigma$ , applied to the boundary of REV. The problem to be solved is the determination of local fields of stress, strain and displacement inside the REV. This problem (P) may be decomposed into two sub-problems in terms of displacement field, as shown in Fig. 3. Accordingly, the macroscopic strain  $\mathbf{E}$  of the cracked medium is written as the sum of two terms

$$\mathbf{E} = \mathbf{E}^s + \mathbf{E}^c \quad (3)$$

The first term corresponds to the solid matrix strain  $\mathbf{E}^s$  and the second term  $\mathbf{E}^c$  is related to the contribution of microcracks, more precisely, of the displacement discontinuities, which reads:

$$\mathbf{E}^c = \mathcal{N} \int_{\omega^+} \underline{n} \otimes \underline{\underline{[u]}} dS = \beta (\underline{n} \otimes \underline{n}) + \underline{\underline{\gamma}} \otimes \underline{n} \quad (4)$$

with  $\beta$  and  $\underline{\underline{\gamma}}$  as two kinetic variables characterizing the crack opening–closure state and the sliding in the crack plane, respectively, which are defined as

$$\beta = \mathcal{N} \int_{\omega^+} [u_n] dS, \quad \underline{\underline{\gamma}} = \int_{\omega^+} [\underline{u}_t] dS \quad (5)$$

with  $[\underline{u}_t] = [\underline{u}] - [u_n] \underline{n}$ .  $\omega^+$  denotes the crack surface with the unit normal  $\underline{n}$ .

The microscopic stress field  $\sigma^s$  is uniform which implies the relation:  $\sigma^s = \langle \sigma^s \rangle_{\Omega} = \Sigma$  and the local stress  $\sigma^c$  on cracks is the self-equilibrating. Finally, the free energy  $W$  is expressed as the sum of an elastic energy corresponding to the solid matrix and of the stored energy due to the local stress field:

$$W = \frac{1}{2} (\mathbf{E} - \mathbf{E}^c) : \mathbb{C}^s : (\mathbf{E} - \mathbf{E}^c) - \frac{1}{2} \mathcal{N} \int_{\omega^+} \{ (\sigma^c - \Sigma) : (\underline{n} \otimes \underline{n}) [u_n] + \underline{n} (\sigma^c - \Sigma) [\underline{u}_t] \} dS \quad (6)$$

In order to establish the relation between the deformation  $\mathbf{E}^c$  and the local stress field  $\sigma^c$  in the cracks, inspired by

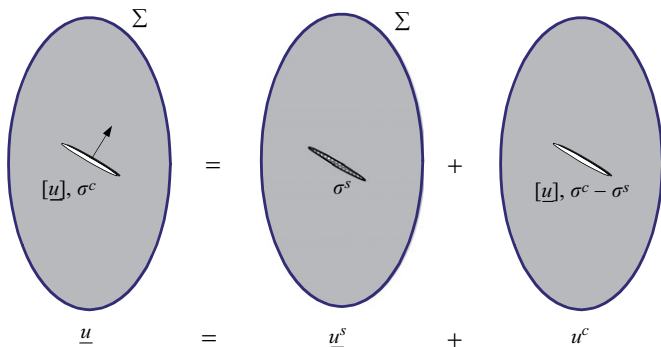


Fig. 3. Problem decomposition in terms of displacement field.

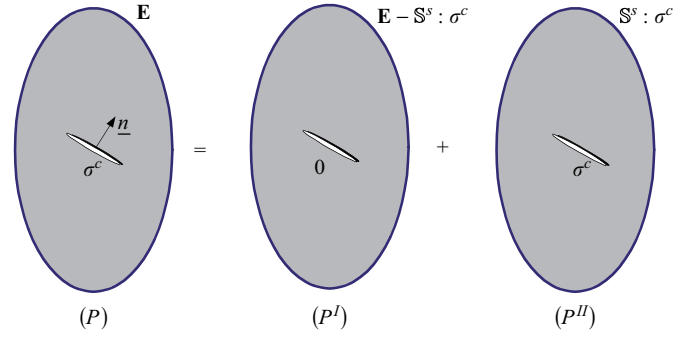


Fig. 4. Homogenization-based problem decomposition.

the work of Barthelemy [35], the initial problem is decomposed into two sub-problems, as shown in Fig. 4.

The solution of the sub-problem  $P^I$  is obtained according to the homogenization procedure:

$$\mathbf{E}^I = \varphi^c \mathbb{A}^c : (\mathbf{E} - \mathbb{S}^s : \sigma^c), \quad \mathbb{S}^s = (\mathbb{C}^s)^{-1}, \quad (7)$$

where  $\mathbb{A}^c$  is the concentration tensor associated with the considered family of microcracks,  $\mathbb{S}^s$  the elastic compliance tensor of solid matrix. In the case of opening cracks ( $\sigma^c = 0$  and  $\beta > 0$ ), the above expression (7) returns to that obtained in the classical homogenization procedure:

$$\mathbf{E}^I = \varphi^c \mathbb{A}^c : \mathbf{E}. \quad (8)$$

The corresponding macroscopic stress is determined with the help of the macroscopic stiffness tensor  $\mathbb{C}^{\text{hom}}$ :

$$\Sigma^I = \mathbb{C}^{\text{hom}} : (\mathbf{E} - \mathbb{S}^s : \sigma^c) \quad (9)$$

for which we recall the general effective stiffness tensor  $\mathbb{C}^{\text{hom}} = \mathbb{C}^s + \varphi^c (\mathbb{C}^c - \mathbb{C}^s) : \mathbb{A}^c$  in the case of open cracks ( $\mathbb{C}^c = 0$ ) and frictionless closed cracks ( $\mathbb{C}^c = 3k^s \mathbb{J}$ ). Further, the uniformity of the sub-problem  $P^{II}$  gives:

$$\Sigma = \Sigma^I + \sigma^c. \quad (10)$$

The coherence between the expressions (7) and (4) leads to the equality  $\mathbf{E}^I = \mathbf{E}^c$ , i.e.:

$$\beta (\underline{n} \otimes \underline{n}) + \underline{\underline{\gamma}} \otimes \underline{n} = \varphi^c \mathbb{A}^c : (\mathbf{E} - \mathbb{S}^s : \sigma^c), \quad (11)$$

which allows us to simplify the notation through replacing  $\mathbf{E}^c$  and  $\mathbf{E}^I$  by  $\mathbf{E}^{\text{pl}}$ . The combination of Eqs. (7), (9) and (10) allows expressing the local stress field  $\sigma^c$  as a function of the macroscopic stress  $\Sigma$  and of the crack induced inelastic deformation  $\mathbf{E}^{\text{pl}}$ :

$$\sigma^c = \Sigma - \mathbb{C}^{\text{pl}} : \mathbf{E}^{\text{pl}} \quad (12)$$

with

$$\mathbb{C}^{\text{pl}} = [\varphi^c \mathbb{A}^c : (\mathbb{I} - \varphi^c \mathbb{A}^c)^{-1} : \mathbb{S}^s]^{-1}. \quad (13)$$

Eq. (12) can also be rewritten in the form

$$\sigma^c - \Sigma = -\mathbb{C}^{\text{pl}} : \mathbf{E}^{\text{pl}}. \quad (14)$$

Insertion of Eq. (14) into Eq. (6) and using Eq. (4) gives the free energy function of the cracked material:

$$W = \frac{1}{2}(\mathbf{E} - \mathbf{E}^{\text{pl}}) : \mathbb{C}^s : (\mathbf{E} - \mathbf{E}^{\text{pl}}) + \frac{1}{2}\mathbf{E}^{\text{pl}} : \mathbb{C}^{\text{pl}} : \mathbf{E}^{\text{pl}}. \quad (15)$$

### 3. Formulation of anisotropic damage model

#### 3.1. Constitutive equations

Based on the background previously defined, the formulation of a micromechanical model for anisotropic damage is given in this section. Due to the simplicity of the stress-based formulation in the case of Mori–Tanaka estimate [28], we are interested in the associated free enthalpy (Gibbs free energy) function,  $W^*$ , which can be obtained by Legendre–Fenchel transform of  $W$ . Using the following strain concentration tensor corresponding to the Mori–Tanaka estimate [28,36,37]:

$$\mathbb{A}^c = (\mathbb{I} + \mathbb{S}_\varepsilon)^{-1} : [\varphi^s \mathbb{I} + \varphi^c (\mathbb{I} + \mathbb{S}_\varepsilon)]^{-1}, \quad (16)$$

where  $\mathbb{S}_\varepsilon$  is the Eshelby tensor with components given in [23,24], the free enthalpy  $W^*$  is then expressed in the following form:

$$W^* = \frac{1}{2} \Sigma : \mathbb{S}^s : \Sigma + \beta \Sigma : (\underline{n} \otimes \underline{n}) + \underline{\gamma} \cdot \Sigma \cdot \underline{n} - \frac{1}{2d} [H_0 \beta^2 + H_1 \underline{\gamma} \cdot \underline{\gamma}] \quad (17)$$

with  $H_0 = 3E^s/16[1 - (v^s)^2]$  and  $H_1 = H_0(1 - v^s/2)$ .

The above relations are developed for a single family of microcracks. They can be extended to any distribution of microcracks. For this, however, some assumptions should be precised. In the present model, for the sake of simplicity, we neglect the interaction between cracks and consider a continuous space distribution of cracks. Accordingly, the macroscopic Gibbs free energy, denoted,  $\Psi^*$ , is obtained by integration of  $W^*$  on the unit sphere  $\mathcal{S}^2 = \{\underline{n}, |\underline{n}| = 1\}$ :

$$\begin{aligned} \Psi^* &= \frac{1}{2} \Sigma : \mathbb{S}^s : \Sigma \\ &+ \Sigma : \frac{1}{4\pi} \int_{\mathcal{S}^2} [\beta(\underline{n})(\underline{n} \otimes \underline{n}) + \underline{\gamma}(\underline{n}) \otimes \underline{n}] dS \\ &- \frac{1}{2} \frac{1}{4\pi} \int_{\mathcal{S}^2} \frac{1}{d(\underline{n})} [H_0 \beta^2(\underline{n}) + H_1 \underline{\gamma}^2(\underline{n})] dS. \end{aligned} \quad (18)$$

Since the distributions  $\beta(\underline{n})$ ,  $\underline{\gamma}(\underline{n})$  and  $d(\underline{n})$  are generally unknown, the analytical form of  $\Psi^*$  is not available. Hence, the Gauss type numerical integration formula with  $N$  points is adopted in this study, similarly to [38]. Therefore, the integral form (18) is approximated by the following addition procedure:

$$\begin{aligned} \Psi^* &= \frac{1}{2} \Sigma : \mathbb{S}^s : \Sigma + \Sigma : \sum_{r=1}^N w^r [\beta^r(\underline{n}^r \otimes \underline{n}^r) + \underline{\gamma}^r \otimes \underline{n}^r] \\ &- \frac{1}{2} \sum_{r=1}^N \frac{w^r}{d^r} [H_0 (\beta^r)^2 + H_1 \underline{\gamma}^r \cdot \underline{\gamma}^r], \end{aligned} \quad (19)$$

where  $w^r$  is the weighting coefficient associated with the  $r$ th crack family characterized by the unit vector  $\underline{n}^r$ .

The standard thermodynamics framework is now invoked. The microscopic thermodynamic force associated with the internal variable  $\mathbf{E}^{\text{pl}}$  corresponding to any family of cracks, noted by  $\mathbf{F}^{\text{pl}}$ , is derived from the differentiation of Eq. (15):

$$\mathbf{F}^{\text{pl}} = - \frac{\partial W}{\partial \mathbf{E}^{\text{pl}}} = \Sigma - \mathbb{C}^{\text{pl}} : \mathbf{E}^{\text{pl}} = \sigma^c \quad (20)$$

In a similar way,  $F^\beta$  and  $F^\gamma$  associated forces respectively with  $\beta$  and  $\underline{\gamma}$  are given by

$$F^\beta = - \frac{\partial W}{\partial \beta} = \sigma^c : (\underline{n} \otimes \underline{n}), \quad (21)$$

$$F^\gamma = - \frac{\partial W}{\partial \underline{\gamma}} = \sigma^c \underline{n} (\delta - \underline{n} \otimes \underline{n}). \quad (22)$$

As previously mentioned in Eq. (2), the crack opening/closure transition condition is defined by

$$\sigma^c : (\underline{n} \otimes \underline{n}) = 0 \quad \text{or} \quad F^\beta = 0, \quad (23)$$

which leads to the following relation for the Mori–Tanaka scheme:

$$\beta = \frac{d}{H_0} \Sigma : (\underline{n} \otimes \underline{n}). \quad (24)$$

Moreover, using the condition  $F^\gamma = 0$  provides the following expression:

$$\underline{\gamma} = \frac{d}{H_1} \Sigma \underline{n} (\delta - \underline{n} \otimes \underline{n}). \quad (25)$$

Taking into account the unilateral condition, a clear distinction between the opened cracks families, numbered  $N_o$ , and the closed cracks families,  $N_c$ , is needed. Substitution of Eqs. (24) and (25) into Eq. (19) yields the expression:

$$\begin{aligned} \Psi^* &= \frac{1}{2} \Sigma : \mathbb{S}^s : \Sigma + \frac{1}{2} \Sigma : \sum_{r=1}^{N_o} w^r d^r \left( \frac{1}{H_0} \mathbb{E}^{2,r} + \frac{1}{2H_1} \mathbb{E}^{4,r} \right) : \Sigma \\ &+ \Sigma : \sum_{r=1}^{N_c} w^r [\beta^r(\underline{n}^r \otimes \underline{n}^r) + \underline{\gamma}^r \otimes \underline{n}^r] - \frac{1}{2} \sum_{r=1}^{N_c} \frac{w^r}{d^r} [H_0 (\beta^r)^2 + H_1 \underline{\gamma}^r \cdot \underline{\gamma}^r] \end{aligned} \quad (26)$$

with the notation  $\Delta^r = \underline{n}^r \otimes \underline{n}^r$ ,  $\mathbb{E}^{2,r} = \Delta^r \otimes \Delta^r$  and  $\mathbb{E}^{4,r} = \frac{1}{2} [\Delta^r \otimes \otimes (\delta - \Delta^r) + (\delta - \Delta^r) \otimes \otimes \Delta^r]$ .

The first state law can be now derived from the macroscopic Gibbs energy (26), which defines the macroscopic stress–strain relations:

$$\begin{aligned} \mathbf{E} &= \mathbb{S}^s : \Sigma + \sum_{r=1}^{N_o} w^r d^r \left( \frac{1}{H_0} \mathbb{E}^{2,r} + \frac{1}{2H_1} \mathbb{E}^{4,r} \right) : \Sigma \\ &+ \sum_{r=1}^{N_c} w^r [\beta^r(\underline{n}^r \otimes \underline{n}^r) + \underline{\gamma}^r \otimes \underline{n}^r]. \end{aligned} \quad (27)$$

The thermodynamic force associated with any  $d^r$  is defined as  $F^{d^r} = \partial\Psi^*/\partial d^r$ . We obtain for the family of open cracks:

$$F^{d^r} = \frac{1}{2}\Sigma : \left( \frac{1}{H_0} \mathbb{E}^{2,r} + \frac{1}{2H_1} \mathbb{E}^{4,r} \right) : \Sigma \quad (28)$$

and, equivalently:

$$F^{d^r} = \frac{1}{2(d^r)^2} \left[ H_0(\beta^r)^2 + H_1 \underline{\gamma}^r \cdot \underline{\gamma}^r \right] \quad (29)$$

for the family of closed cracks. We can see that it is needed to determine the variables associated with each family of microcracks, namely  $\beta^r, \underline{\gamma}^r, d^r$ .

### 3.2. Friction–damage coupling and evolution laws

To complete the formulation of damage model, we need to determine the evolution laws of damage and frictional sliding. We assume that the closed frictional cracks obey the classical Coulomb criterion at local scale and that the saturation of the criterion is uniform on the crack faces. At the microscopic scale, the Coulomb criterion  $g(\sigma^c) = 0$  is determined by means of normal and tangential component of the local stress  $\sigma^c$  applied on the crack:

$$g = |\sigma^c \underline{n}(\delta - \underline{n} \otimes \underline{n})| + \mu_c \sigma^c : (\underline{n} \otimes \underline{n}) = 0, \quad (30)$$

where  $\mu_c$  is the friction coefficient on the cracks faces. In terms of the thermodynamic forces  $F^\beta$  and  $\underline{F}^\gamma$ , this criterion also reads:

$$g(\sigma^c) = |\underline{F}^\gamma| + \mu_c F^\beta = 0 \quad (31)$$

From this criterion, the pressure sensitivity of rock behavior is taken into account through the effect of normal stress on the crack  $\sigma^c : (\underline{n} \otimes \underline{n})$  or equivalently  $F^\beta$ . Note that a Coulomb-type criterion without cohesion term is here used at the (microscopic) local scale for closed microcracks under compressive stress. In this case, the frictional term is dominant regarding the cohesion term. Further, the use of a criterion without cohesion at the microscopic scale does not mean that the macroscopic tensile strength of material is zero. Indeed, the macroscopic tensile strength is determined by material resistance to damage related to propagation of open cracks.

Concerning the damage evolution law, the following general form is here adopted for the damage criterion of each family of microcracks:

$$f(F^d, d) = F^d - \mathcal{R}(d) = 0. \quad (32)$$

The function  $\mathcal{R}(d)$  represents the material resistance to the damage evolution by growth of microcracks, which can be a priori determined from experimental investigations. For the sake of simplicity, we consider here a linear function in  $d$ , as initially proposed in [39] in the context of macroscopic modeling of isotropic damage:

$$\mathcal{R}(d) = c_0 + c_1 d, \quad (33)$$

where  $c_0$  and  $c_1$  are two model's parameters, respectively, defining the initial damage threshold and kinetics of damage evolution. These parameters may be identified from experimental data showing progressive degradation of elastic properties during unloading cycles in triaxial compression tests. Note that the damage criterion used in this paper is formulated in the framework of irreversible thermodynamics applied to the microscopic scale. The damage conjugate force is equivalent to strain energy release rate used in fracture mechanics. The determination of a fully micromechanics-based damage evolution law is still an open issue to be performed in future development.

The evolution rates of damage variable  $d$  and of sliding vector  $\underline{\gamma}$  can be determined using the standard normality rule:

$$\dot{d} = \dot{\lambda}^d \frac{\partial f(F^d, d)}{\partial F^d} = \dot{\lambda}^d, \quad (34)$$

$$\dot{\underline{\gamma}} = \dot{\lambda}^\gamma \frac{\partial g}{\partial \underline{F}^\gamma} = \dot{\lambda}^\gamma \underline{\nu}, \quad (35)$$

where  $\dot{\lambda}^d$  and  $\dot{\lambda}^\gamma$  are the multipliers associated with damage and frictional sliding, respectively, which are determined by the consistency conditions  $\dot{f} = 0$  and  $\dot{g} = 0$ . The unit vector  $\underline{\nu}$  represents the direction of frictional sliding, defined by  $\underline{F}^\gamma / |\underline{F}^\gamma|$ . For the evolution of the variable  $\beta$ , which represents the normal opening due to frictional sliding of microcracks, two different situations can be considered:

- (a) In the case of frictional sliding without dilatation in smooth cracks, we have  $\dot{\beta} = 0$ , which implies a non-associated flow rule for inelastic deformation  $\mathbf{E}^{pl}$ .
- (b) For the case of frictional sliding with normal dilation in cracks with rough faces, we have  $\dot{\beta} \neq 0$ . For simplicity, we adopt here a normality flow rule for the evolution of  $\mathbf{E}^{pl}$  which leads to the relation:

$$\dot{\beta} = \mu_c \dot{\lambda}^\gamma \quad (36)$$

Note that an associated flow rule is here adopted for frictional sliding. The advantage of this choice consists in the symmetric property of the homogenized compliance tensor  $\mathbb{S}_t^{hom}$ . However, there is no difficulty to take a non-associated flow rule in the formulation, for instance by introducing a dilatancy coefficient different with the frictional coefficient.

## 4. Computational aspects and numerical implementation

We are interested now in implementing the proposed damage–friction coupled model into the finite element software Abaqus by means of the provided user subroutine UMAT which authorizes to define the mechanical constitutive behaviour of a material. In UMAT, the material Jacobian matrix,  $\partial\Sigma/\partial E$ , must be provided for the mechanical constitutive model and the values of stresses

and solution-dependent state variables (namely the variables  $d^r$ ,  $\beta^r$  and  $\underline{\gamma}^r$  in this study) at the end of the increment must be updated. For this purpose, it is necessary to determine the rate form of the macroscopic stress–strain relation which provides the consistent tangent operator and to develop the local integration of the proposed model.

#### 4.1. Determination of the tangent matrix

For the sake of simplicity, the strategy that we adopt is, according to the macroscopic stress–strain relation defined in Eq. (27), to express the macroscopic strain increment  $\dot{E}$  as a function of the stress one:

$$\dot{E} = \mathbb{S}_i^{\text{hom}} : \dot{\Sigma} \quad (37)$$

The Jacobian matrix can be obtained by an inverse calculation of  $\mathbb{S}_i^{\text{hom}}$  [28]. For a given family of closed microcracks, if the damage growth and friction sliding criteria are simultaneously verified, the corresponding consistence conditions are written as follows:

$$\begin{cases} \frac{\partial g}{\partial \Sigma} : \dot{\Sigma} + \frac{\partial g}{\partial \underline{\gamma}} \dot{\underline{\gamma}} + \frac{\partial g}{\partial \beta} \dot{\beta} + \frac{\partial g}{\partial d} \dot{d} = 0, \\ \frac{\partial f}{\partial \underline{\gamma}} \dot{\underline{\gamma}} + \frac{\partial f}{\partial \beta} \dot{\beta} + \frac{\partial f}{\partial d} \dot{d} = 0. \end{cases} \quad (38)$$

And for a given family of opened microcracks, the consistence condition for damage evolution reads:

$$\frac{\partial f}{\partial \Sigma} : \dot{\Sigma} + \frac{\partial f}{\partial d} \dot{d} = 0. \quad (39)$$

Considering the relations (38) and (39), respectively, for the families of closed and opened cracks, as well as the rate form of Eq. (27), the tangent operator  $\mathbb{S}_i^{\text{hom}}$  is written in the following form:

$$\begin{aligned} \mathbb{S}_i^{\text{hom}} = & \mathbb{S}^s + \frac{1}{c_1} \sum_{r=1}^{N_o} \langle f^r \rangle \omega^r \frac{\partial f^r}{\partial \Sigma} \otimes \frac{\partial f^r}{\partial \Sigma} \\ & + \sum_{r=1}^{N_c} \langle g^r \rangle \omega^r \frac{d^r}{\tilde{H}_\gamma} \frac{\partial g^r}{\partial \Sigma} \otimes \frac{\partial g^r}{\partial \Sigma} \end{aligned} \quad (40)$$

with  $f^r$  the damage function of  $r$ th family of microcracks.

$$\begin{aligned} \frac{\partial f^r}{\partial \Sigma} = & \left( \frac{1}{H_0} \mathbb{E}^{2,r} + \frac{1}{2H_1} \mathbb{E}^{4,r} \right) : \Sigma, \quad \frac{\partial g^r}{\partial \Sigma} \\ = & \underline{\nu}^r \otimes \underline{n}^r + \mu_c \underline{n}^r \otimes \underline{n}^r, \end{aligned}$$

and

$$\tilde{H}_\gamma = H_1 + \mu_c^2 H_0 - \frac{\langle f^r \rangle (\mu_c H_0 \beta^r + H_1 \underline{\gamma}^r \underline{\nu}^r)^2}{H_0 (\beta^r)^2 + H_1 \underline{\gamma}^r \underline{\gamma}^r + c_1 (d^r)^3},$$

where  $\langle x \rangle = 1$  when  $x > 0$ , and zero otherwise.

#### 4.2. Local integration of model

Considering the requirements of the user subroutine UMAT in Abaqus, an incremental procedure associated

with the rate form of stress–strain relation is used based on the strain discretization of the considered loading path. Furthermore, a widely used prediction–correction splitting scheme is adopted considering the strongly non linear character of constitutive law. The scheme from the step  $j$  to  $j+1$  is briefly summarized below:

#### (1) Elastic prediction:

For each family of microcracks, put  $d_{j+1} = d_j$ ,  $\beta_{j+1} = \beta_j$ ,  $\underline{\gamma}_{j+1} = \underline{\gamma}_j$ ;

calculate  $E_j^e = E_j - \sum_{r=1}^N \omega^r \left( \beta^r \underline{n}^r \otimes \underline{n}^r + \underline{\gamma}^r \otimes \underline{n}^r \right)$ ,

then  $E_{j+1}^e = E_j^e + \Delta E_{j+1}$  and  $\Sigma_{j+1} = \mathbb{C}^s : E_{j+1}^e$ .

Examine the opening-closure condition for each family:  $F^{\beta^r} = \Sigma_{j+1} : (\underline{n}^r \otimes \underline{n}^r) - \frac{H_0}{d_j^r} \beta_j^r$

Determination of increments  $\Delta d_{j+1}^r$ ,  $\Delta \underline{\gamma}_{j+1}^r$  and  $\Delta \beta_{j+1}^r$ :  $F^{\beta^r} > 0$ : calculate  $\Delta d_{j+1}^r$  using Eqs. (32) and (28) for open cracks;  $F^{\beta^r} \leq 0$ : examine the frictional sliding criterion (30) for closed cracks:

$$\begin{cases} \text{if } g < 0, \text{ then } \Delta d_{j+1}^r = 0, \Delta \underline{\gamma}_{j+1}^r = 0, \Delta \beta_{j+1}^r = 0, \\ \text{if } g \geq 0, \text{ calculate } \Delta \underline{\gamma}_{j+1}^r, \Delta \beta_{j+1}^r \text{ using Eq. (31),} \\ \text{calculate } f^r : \begin{cases} \text{if } f^r < 0, \text{ then } \Delta d_{j+1}^r = 0; \\ \text{or calculate } \Delta d_{j+1}^r \text{ using Eq. (39).} \end{cases} \end{cases}$$

#### (2) Update the variables:

$$d_{j+1}^r = d_j^r + \Delta d_{j+1}^r,$$

$$\underline{\gamma}_{j+1}^r = \underline{\gamma}_j^r + \Delta \underline{\gamma}_{j+1}^r,$$

$$\beta_{j+1}^r = \beta_j^r + \Delta \beta_{j+1}^r.$$

#### (3) Update the stress tensor:

Calculate  $\Sigma_{j+1}$ .

Note that the inverse tensors involved in the Eshelby solutions (see Eq. (16)) can be easily calculated using the Walpole's tensorial decomposition algebra [40]. Yang et al. [41] have proposed an analytical solution for penny-shaped inhomogeneities in terms of global Eshelby's tensor. This could also be helpful to simplify the calculation.

### 5. Validation and numerical simulations

In this section, the proposed model will be used to simulate conventional and true triaxial compression tests on two granites, respectively, from Lac du Bonnet in Canada and Westerly in USA. The proposed micromechanical model contains only six parameters and each has a clear physical meaning. The initial elastic constants  $E_0$  and

$v_0$  can be determined from linear part of idealized stress-strain curve in a triaxial compression test. The parameters  $c_0$  and  $c_1$  are involved in the damage criterion. These parameters may be determined by evaluating progressive degradation of elastic modulus on unloading stress strain curves. The friction coefficient  $\mu_c$  may be evaluating by comparing mechanical responses with different confining pressures. The initial overall density of microcracks distribution is assumed to be isotropic and characterized by  $d_0$ . Its value could be determined from hydrostatic compression test of rock.

5.1. Simulations of conventional triaxial compression tests

The predictive capacity of constitutive models is first checked through the simulation of conventional triaxial compression tests under different confining pressures. In these tests, the cylinder samples are first subjected to a hydrostatic stress called confining pressure. Then the axial stress ( $\Sigma_{11}$ ) is increased while the lateral stress (confining pressure,  $\Sigma_{22} = \Sigma_{33}$ ) is kept constant. The considered material is the so-called Lac du Bonnet granite largely studied in the underground research laboratory for nuclear waste storage in Canada [42–44]. The following values of parameters are used for simulation:  $E^s = 68000$  MPa,  $\nu^s = 0.21$ ,  $c_0 = 3 \times 10^{-3} \text{ J m}^{-2}$ ,  $c_1 = 6 \times 10^{-2} \text{ J m}^{-2}$ ,  $d_0 = 1 \times 10^{-3}$ ,  $c_1 = 6 \times 10^{-2} \text{ J m}^{-2}$ ,  $d_0 = 1 \times 10^{-3}$ ,  $\mu_c = 0.7$ . The procedure for the parameter identification from conventional rock mechanics tests is detailed in [28]. The comparisons of the stress–strain relations between the experimental data and model predictions are shown in Figs. 5–7 (axial strain  $E_{11}$  [%] in the direction of axis of cylinder sample, lateral strain  $E_{22} = E_{33}$  [%] and volumetric strain  $E_v = E_{11} + 2E_{33}$  [%]). We can see that the main features of brittle rock behaviour, previously mentioned, are correctly described by the model. Moreover, comparisons of numerical predictions between the models with and without friction-related dilation are also presented. It is clearly shown that the model with dilatation gives a much better prediction than the model without dilation. The macroscopic volumetric dilatancy of brittle

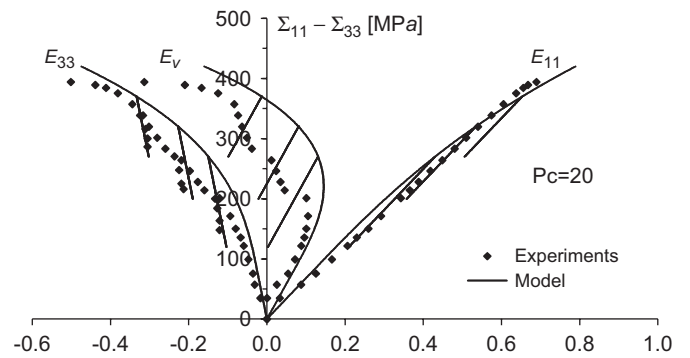


Fig. 6. Comparisons between data and model's predictions for a triaxial compression cyclic test with confining pressure of 20 MPa using the model with frictional dilation.

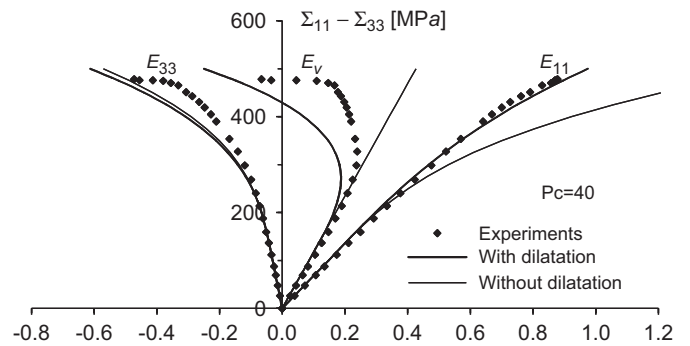


Fig. 7. Comparisons between data and model's predictions for a triaxial compression test with confining pressure of 40 MPa using the models with and without frictional dilation.

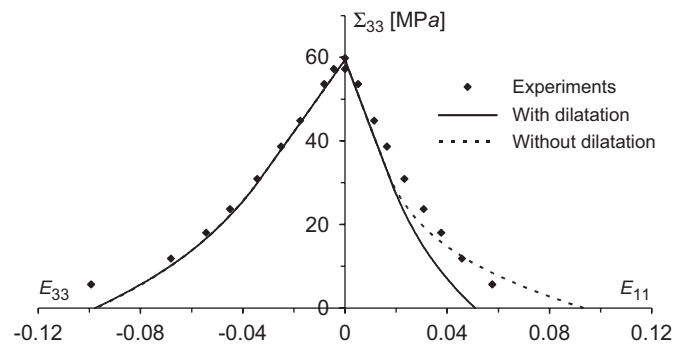


Fig. 8. Comparison between data and model's prediction for a lateral extension test.

rocks is physically related to the microscopic normal dilation during frictional sliding along microcracks. In Fig. 6, some unloading paths are shown. As the microcracks are closed due to compressive stress and due to that fact that the crack sliding is locked by frictional effect, we obtain linear elastic response during unloading of deviatoric stress.

Fig. 8 shows the simulation of a lateral extension test. In this kind of tests, the rock sample is first submitted to a hydrostatic stress, for instance  $\Sigma_{11} = \Sigma_{22} = \Sigma_{33} = 60$  MPa

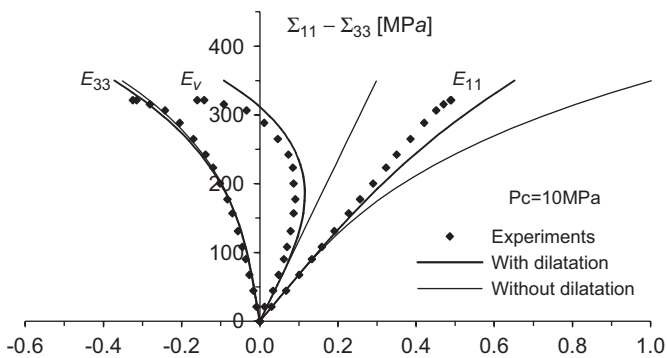


Fig. 5. Comparison between data and model's predictions for a triaxial compression test with confining pressure of 10 MPa using the models with and without frictional dilation.

for the test shown in Fig. 8. The axial stress  $\Sigma_{11}$  is increased in a second stage to a prescribed value, for instance  $\Sigma_{11} = 160$  MPa for the test shown in Fig. 8. In the last stage, the confining pressure ( $\Sigma_{22} = \Sigma_{33}$ ) is progressively reduced from 60 MPa to zero while the axial stress is kept constant at 160 MPa. Conventionally, only the stress–strain curves during the last stage are presented for the lateral extension test as shown in Fig. 8. Note that this test is largely performed in rock mechanics because it approximately reproduces the stress path near the surface of cavity during excavation in axi-symmetrical conditions. From Fig. 8, one can see that a good agreement is obtained between test data and model's predictions. Further, it is noted that the difference in this case is small between the models with and without dilation.

5.2. Simulations of true triaxial compression tests

The simulations of conventional triaxial compression tests provide a first validation of the model in the particular case of axi-symmetrical loading. In order to check the performance of the model in general loading conditions, further validation is needed. In this study, we propose to compare numerical predictions and experimental data for true triaxial compression tests performed on Westerly granite (USA) by Haimson and Chang [45]. The tests were performed on cubic specimens by independently controlling three principal stresses in three axes. The identification of parameters is made on a conventional triaxial compression test with a confining pressure of 60 MPa. The

following values are obtained:  $E^s = 68\,000$  MPa,  $v^s = 0.21$ ,  $c_0 = 3 \times 10^{-3} \text{ J m}^{-2}$ ,  $c_1 = 0.18 \text{ J m}^{-2}$ ,  $d_0 = 1 \times 10^{-3}$ ,  $\mu_c = 0.7$ .

The loading path applied to true triaxial test is composed of three phases: (i) a hydrostatic compression phase until 60 MPa; (ii)  $\Sigma_{33}$  being kept constant (60 MPa) and increasing  $\Sigma_{11} = \Sigma_{22}$  to the prescribed values of 60, 113, 180 and 249 MPa; and (iii) the value of  $\Sigma_{22}$  and  $\Sigma_{33}$  being hold constant and the value of  $\Sigma_{11}$  increased from  $\Sigma_{11} = \Sigma_{22}$  to prescribed values of 747, 822, 860, and 861 MPa. The proposed micromechanical model is now applied to simulate these tests. Comparisons between the model's predictions and test data are shown in Fig. 9 and one can see a good agreement for different loading paths.

Compared with phenomenological models, the micro-mechanical model is able to provide not only overall stress–strain responses but also the distribution of crack density parameter. Fig. 10 shows three-dimensional damage density distributions with the different intermediate principal stress value  $\Sigma_{22}$ . Noting  $o$  as the original point in the considered space and  $a$  as a point on the surfaces of distribution functions, the orientation of the vector  $\vec{oa}$  corresponds to the family of microcracks with unit normal  $\vec{oa}/\|\vec{oa}\|$  and the damage density is evaluated by  $\|\vec{oa}\|$ . We notice that as  $\Sigma_{22}$  increases from 60 to 249 MPa, the growth of damage in the planes 1–2 is progressively blocked. In addition, the greatest value always occurs in the planes 1–3 and the dip angles for all the four tests are always about  $62^\circ$ . This value is slightly different from the experimental data (ranging from  $67^\circ$  to  $72^\circ$ ) reported in

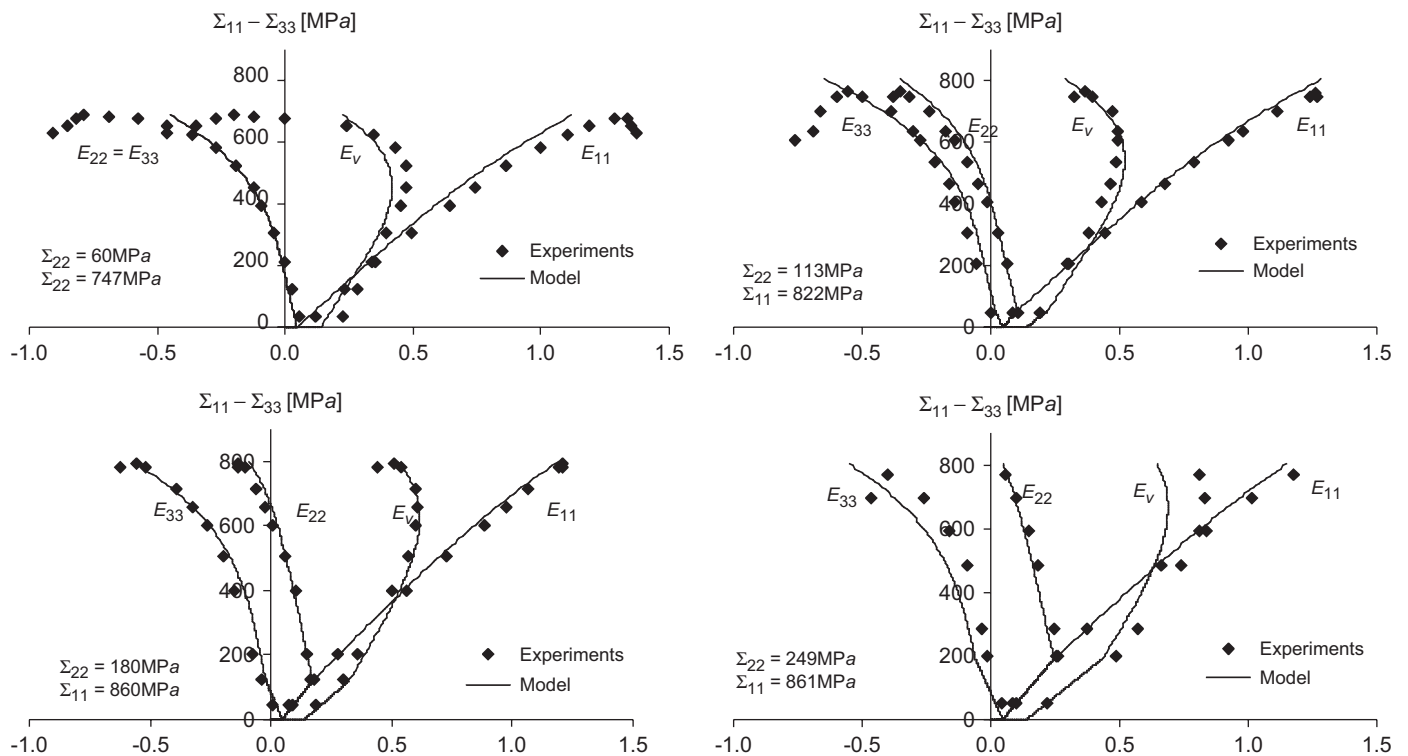


Fig. 9. Comparisons of model's predictions with experimental data for true triaxial compression tests on Westerly granite [43].

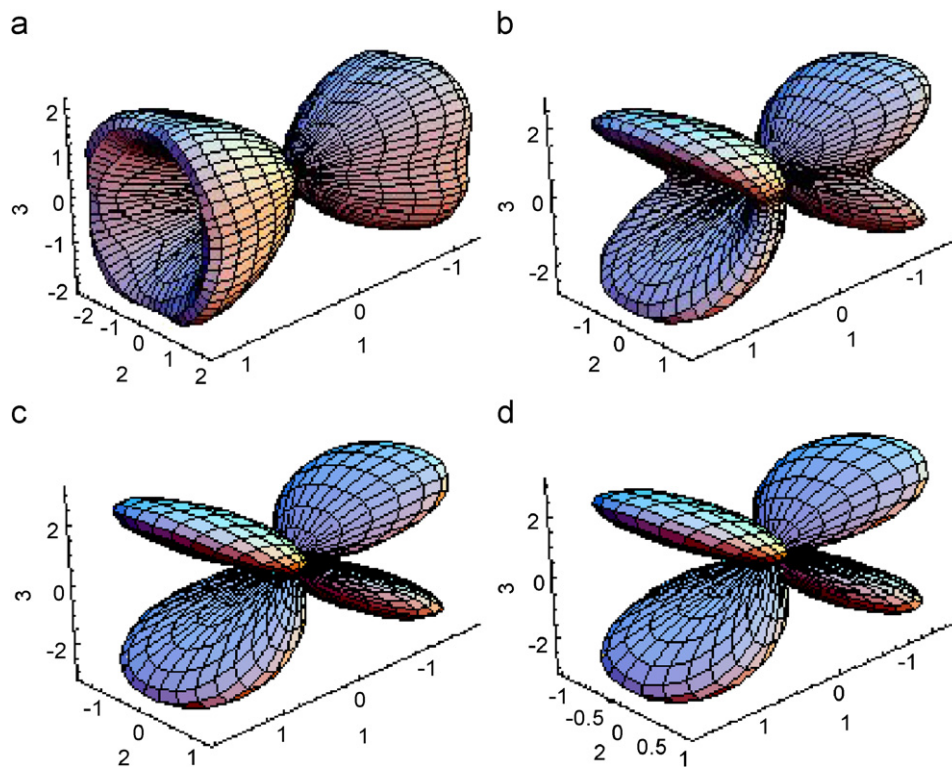


Fig. 10. Damage density distributions in true triaxial compression tests on Westerly granite: (a)  $\Sigma_{22} = 60$  MPa,  $\Sigma_{11} = 747$  MPa; (b)  $\Sigma_{22} = 113$  MPa,  $\Sigma_{11} = 822$  MPa; (c)  $\Sigma_{22} = 180$  MPa,  $\Sigma_{11} = 860$  MPa; (d)  $\Sigma_{22} = 249$  MPa,  $\Sigma_{11} = 861$  MPa.

[45]. This difference may be explained by the fact that the frictional sliding criterion (30) is an interfacial one and thus the intermediate stress  $\Sigma_{22}$  cannot be taken into account for the microcracks with the normal vectors within the planes 1–3.

## 6. Application to the ACEL's mine-by experiment

After the simulation of laboratory tests, in this section, we will discuss the feasibility of applying the micromechanical model to engineering problems. We propose to study mechanical responses induced by the excavation of a 3.5 m diameter circular tunnel in the context of the Underground Research Laboratory for nuclear waste storage (URL-ACEL Canada). The mine-by experiment was conducted at the 420 m level in order to investigate rock damage process during excavation by the use of a non-explosive technique [42,44,46]. The tunnel is subjected to a strongly deviatoric initial stress state as shown in Fig. 10. Radial displacement evolution and acoustic emission have been monitored. Further, in situ observations have shown two cracked zones in the direction of minor principal stress (see Fig. 11). It has been also observed that the size of cracked zones as well as radial displacement evolve in time due to time dependent behaviour. However, in this work, only short-term behaviour is investigated.

The initial in situ stress state is defined by three principal stresses as follows:  $\sigma_1 = 55$  MPa,  $\sigma_2 = 14$  MPa,  $\sigma_3 = 48$  MPa. The tunnel axis is quasi parallel to the inter-

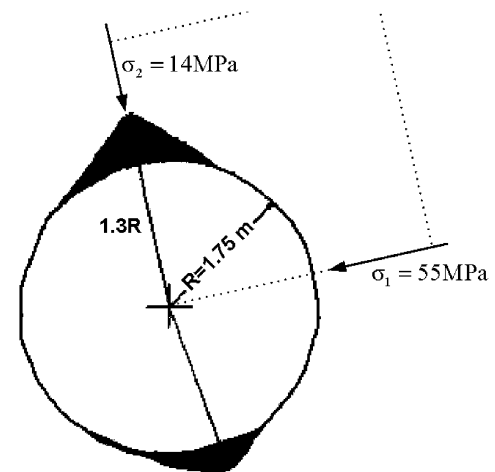


Fig. 11. Observation of cracked zones around the tunnel [44].

mediate principal stress direction. Therefore, 2D modelling has been performed using plane strain conditions. Due to the symmetry of the problem with respect to two principal stresses, only a quarter of domain is considered. The studied region with the outer boundary of  $30 \times 30$  m wide was meshed with 900 rectangle elements. The excavation process is simulated by reducing the normal stress on the tunnel wall from its initial value to the atmospheric pressure. The parameters used for the FEM modelling are determined from a uniaxial compression test on the Lac du Bonnet granite. In Fig. 12, the distribution of damage

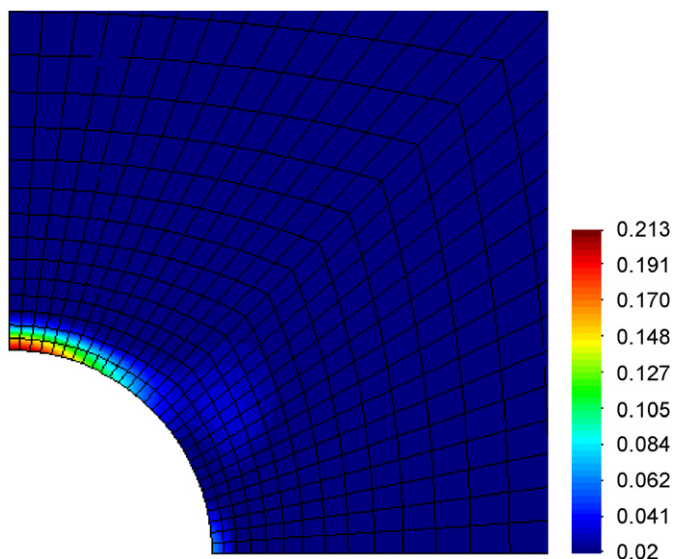


Fig. 12. Distributions of damaged zone.

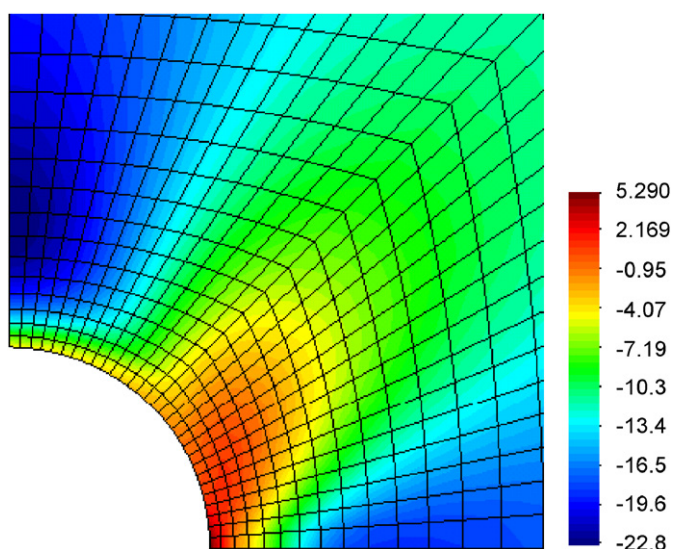


Fig. 13. Distributions of principal stress  $\Sigma_1$ .

density around the tunnel is shown. We can see that the induced damage zone is localized on the top point of the tunnel along the minor principal stress. This is qualitatively in agreement with in situ observations. The predicted size of damaged zone is also close to that observed in place, varying between 0.43 and 0.52 m [46]. Further, tensile stresses have been obtained in numerical predictions in some zones near the tunnel wall (see Fig. 13). However, the magnitude of the maximum tensile stress (5.3 MPa) is quite small and less than the tensile strength of material, which is about 10 MPa. Therefore, the damage is essentially induced by closed cracks due to compressive stresses; and the principal mechanism is frictional sliding along cracks coupled with crack propagation and dilation.

In Fig. 14, we show the radial displacements (convergence) on the tunnel wall in different orientations ( $0^\circ$

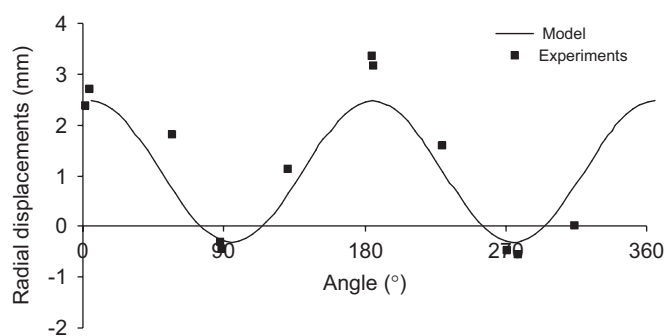


Fig. 14. Comparisons of radial convergence between in situ measurement and model prediction.

corresponds to the direction of major stress). The in situ data are obtained by extensometers placed around the tunnel. We can see good qualitative agreement between the predicted results and in situ data.

## 7. Conclusions

A new micromechanical model is proposed for description of induced anisotropic damage in brittle rocks. Compared with direct approaches based on the theory of linear fracture mechanics, the present model is formulated within a rigorous micro-macro framework using a general procedure of homogenization of heterogeneous media, together with a clear thermodynamics consideration for irreversible dissipation mechanisms. Main features of mechanical behaviours in brittle rocks have taken into account, such as non-linear stress strain relations, volumetric dilatancy, coupling between crack propagation and frictional sliding. The proposed model contains a small number of parameters and each one is related to a physical meaning. The model is then applied to two granites and a good agreement between model's predictions and experimental data for various loading paths is obtained. The proposed model is implemented into a standard FEM code. An example of application has been presented to show the applicability of the micromechanical model to engineering problems. The extension of the model will include, for instance, the determination of a strain localization criterion for modelling of failure process zone, description of correlation between induced damage and variation of permeability, time dependent behaviour due to sub-critical propagation of microcracks.

## References

- [1] Brace WF, Bombolakis EG. A note on brittle crack growth in compression. *J Geophys Res* 1963;68(12):3709–13.
- [2] Wawersik WR, Brace WF. Post-failure behavior of a granite and diabase. *Rock Mech* 1971;3:61–85.
- [3] Nemat-Nasser S, Horii H. Compression-induced non-planar crack extension with application to splitting, exfoliation and rock-burst. *J Geophys Res* 1982;87(B8):6805–21.

- [4] Wong TF. Micromechanics of faulting in Westerly granite. *Int J Rock Mech Min Sci* 1982;19:49–56.
- [5] Kranz RL. Microcracks in rocks: a review. *Tectonophysics* 1983;100:449–80.
- [6] Stef PS. Crack extension under compressive loading. *Eng Fract Mech* 1984;20(3):463–73.
- [7] Horii H, Nemat-Nasser S. Compression-induced microcrack growth in brittle solids: axial splitting and shear failure. *J Geophys Res* 1985;90(B4):3105–25.
- [8] Martin CD, Chandler NA. The progressive failure of Lac du Bonnet granite. *Int J Rock Mech Min Sci* 1994;31(4):643–59.
- [9] Kamiya T, Tita H, Ishijima Y, Aoki K, Sato T. Permeability in anisotropic granite under hydrostatic compression and triaxial compression including post-failure region. In: Aubertin F, Hassani H, Mitri H, editors. *Proceedings of the second American rock mechanic symposium*. Rotterdam: Balkema; 1996. p. 1643–50.
- [10] Chen Z, Narayan SP, Yang Z, Rahman SS. An experimental investigation of hydraulic behaviours of fractures and joints in granitic rock. *Int J Rock Mech Min Sci* 2000;37:1061–71.
- [11] Souley M, Homand F, Pepa S, Hoxha D. Damage-induced permeability changes in granite: a case example at the URL in Canada. *Int J Rock Mech Min Sci* 2001;38:297–310.
- [12] Bossart P, Meier PM, Moeri A, Trick T, Mayor JC. Geological and hydraulic characterisation of the excavation disturbed zone in the Opalinus Clay of the Mont Terri Rock Laboratory. *Eng Geol* 2002;66:19–38.
- [13] Oda M, Takemura T, Aoki T. Damage growth and permeability change in triaxial compression tests of Inada granite. *Mech Mater* 2002;34:313–31.
- [14] Shao JF, Zhou H, Chau KT. Coupling between anisotropic damage and permeability variation in brittle rocks. *Int J Num Anal Meth Geomech* 2005;29:1231–47.
- [15] Chow CL, June W. An anisotropic theory of elasticity for continuum damage mechanics. *Int J Fract* 1987;33:3–16.
- [16] Ju JW. On energy based coupled elastoplastic damage theories: constitutive modeling and computational aspects. *Int J Solids Struct* 1989;25(7):803–33.
- [17] Lemaitre J. *A course on damage mechanics*. 2nd ed. Berlin: Springer; 1992.
- [18] Chaboche JL. Development of continuum damage mechanics for elastic solids sustaining anisotropic and unilateral damage. *Int J Damage Mech* 1993;2:311–29.
- [19] Murakami S, Kamiya K. Constitutive and damage evolution equations of elastic brittle materials based on irreversible thermodynamics. *Int J Mech Sci* 1996;39(4):473–86.
- [20] Halm D, Dragon A. A model of anisotropic damage by mesocrack growth: unilateral effect. *Int J Damage Mech* 1996;5:384–402.
- [21] Krajcinovic D. *Damage mechanics*. Amsterdam: North-Holland; 1996.
- [22] Swoboda G, Yang Q. An energy-based damage model of geomaterials I and II: deduction of damage evolution laws. *Int J Solids Struct* 1999;36:1735–55.
- [23] Mura T. *Micromechanics of defects in solids*. 2nd ed. The Hague: M Nijhoff Pub.; 1987.
- [24] Nemat-Nasser S, Hori M. *Micromechanics: overall properties of heterogeneous materials*. Amsterdam: North-Holland; 1993.
- [25] Andrieux S, Bamberger Y, Marigo JJ. Un modèle de matériau microfissuré pour les roches et les bétons. *J Mécan Théor Appl* 1986;5(3):471–513.
- [26] Gambarotta L, Lagomarsino S. A microcrack damage model for brittle materials. *Int J Solids Struct* 1993;30(2):177–98.
- [27] Pensée V, Kondo D, Dormieux L. Micromechanical analysis of anisotropic damage in brittle materials. *J Eng Mech ASCE* 2002;128(8):889–97.
- [28] Zhu QZ. *Applications des approches d'homogénéisation à la modélisation tridimensionnelle de l'endommagement des matériaux quasi fragile: formulations, validations et implémentations numériques*. Doctoral thesis (in French), University of Lille I, Lille, France, 2006.
- [29] Mori T, Tanaka K. Averages stress in matrix and average elastic energy of materials with misfitting inclusions. *Acta Metall* 1973;21:571–4.
- [30] Ponte-Castaneda P, Willis JR. The effect of spatial distribution on the behavior of composite materials and cracked media. *J Mech Phys Solids* 1995;43:1919–51.
- [31] Budiansky B, O'Connell JR. Elastic moduli of a cracked solid. *Int J Solids Struct* 1976;12:81–97.
- [32] Eshelby JD. The determination of the elastic field of an ellipsoidal inclusion and related problems. *Proc R Soc London* 1957;A241:375–96.
- [33] Eshelby JD. Elastic inclusions and heterogeneities. In: *Progress in solid mechanics*, Vol. 2. Amsterdam: North Holland Pub; 1961.
- [34] Dormieux L, Kondo D. Poroelasticity and damage theory for cracked media. In: Dormieux L, Ulm FJ, editors. *Applied micromechanics of porous media*. CISM; 2005. p. 153–83.
- [35] Barthelemy JF, Dormieux L, Kondo D. Détermination du comportement macroscopique d'un milieu à fissures frottantes. *C R Méc* 2003;331:77–84.
- [36] Benveniste Y. On the Mori-Tanaka method in cracked bodies. *Mech Res Comm* 1986;13(4):193–201.
- [37] Benveniste Y. A new approach to the application of Mori-Tanaka's theory in composite materials. *Mech Mater* 1987;6:147–57.
- [38] Bazant ZP, Oh BH. Efficient numerical integration on the surface of a sphere. *ZAMM* 1986;66:37–49.
- [39] Marigo JJ. Formulation d'une loi d'endommagement d'un matériau élastique. *Compt Rend Acad Sci Paris II* 1981;292:1309–12.
- [40] Walpole LJ. Elastic behavior of composite materials: theoretical foundations. In: Yih CS, editor. *Advances in applied mechanics*, vol. 21. New York: Academic Press; 1981. p. 169–242.
- [41] Yang Q, Zhou WY, Swoboda G. Asymptotic solutions of penny-shaped inhomogeneities in global Eshelby's tensor. *ASME J Appl Mech* 2001;68:740–50.
- [42] Martin CD, Read RS, Martino JB. Observation of brittle failure around a circular test tunnel. *Int J Rock Mech Min Sci* 1997;34(7):1065–73.
- [43] Shao JF, Hoxha D, Bart M, Homand F, Duveau G, Souley M, Hoteit N. Modelling of induced anisotropic damage in granites. *Int J Rock Mech Min Sci* 1999;36:1001–12.
- [44] Martino JB, Chandler NA. Excavation-induced damage studies at the Underground Research Laboratory. *Int J Rock Mech Min Sci* 2004;41:1413–26.
- [45] Haimson B, Chang C. A new true triaxial cell for testing mechanical properties of rock and its use to determine rock strength and deformability of Westerly granite. *Int J Rock Mech Min Sci* 2000;37:285–96.
- [46] Read RS, Martin CD. Technical summary of AECL's mine-by experiment phase I: excavation response. Report AECL-11311, COG-95-171, 1996.